AIAA 2001–0879

Detached Eddy Simulation of Massively Separated Flows

M. Strelets
Russian Scientific Center "Applied Chemistry", St.-Petersburg.

39th AIAA Aerospace Sciences Meeting and Exhibit
January 8–11, 2001/Reno, NV

Detached Eddy Simulation of Massively Separated Flows

M. Strelets *
Russian Scientific Center "Applied Chemistry", St.-Petersburg.

The paper is an attempt to provide a comprehensive description of the state-of-the-art in the area of Detached-Eddy Simulation (DES) of massively separated turbulent flows. DES is a new approach to treatment of turbulence aimed at the prediction of separated flows at unlimited Reynolds numbers and at a manageable cost in engineering. It soundly combines fine-tuned Reynolds-Averaged Navier-Stokes (RANS) technology in the attached boundary layers and the power of Large-Eddy Simulation (LES) in the separated regions. It is essentially a three-dimensional unsteady approach using a single turbulence model, which functions as a subgrid-scale model in the regions where the grid density is fine enough for an LES, and as a RANS model in regions where it is not. SGS function or LES mode prevails where the grid spacing in all directions is much smaller than the thickness of the turbulent shear layer. The model senses the grid density and adjusts itself to a lower level of mixing, relative to RANS mode and, as a result, unlocks the large scale instabilities of the flow and lets the energy cascade extend to length scales close to the grid spacing. In other regions (primarily attached boundary layers), the model is in RANS mode. The approach is non-zonal, i.e., there is a single velocity and model field, and no issue of smoothness between regions. The computing-cost outcome is favorable enough that challenging separated flows at high Reynolds numbers can be treated quite successfully on the latest personal computers. We present a motivation for and detailed formulation of the DES approach based on both its original version employing the one-equation Spalart-Allmaras (S-A) turbulence model, and a new one, using the k-ω Shear Stress Transport model of Menter (M-SST). Numerical issues in DES are also addressed in terms of both accuracy and efficiency. The credibility of the approach is supported by a set of numerical examples of its application: NACA 0012 airfoil at high (up to 90°) angles of attack, circular cylinder with laminar and turbulent separation, backward-facing step, triangular cylinder in a plane channel, raised airport runway, and a model of the landing gear truck. The DES predictions are compared with experimental data and with RANS solutions.

Introduction

THE DES of turbulence[1] has been suggested as a response to the computational and physical challenges associated with the reliable prediction of massively separated turbulent flows in practical geometries at practical Reynolds numbers. Recent estimates for the cost of LES of an airplane or an automobile[2] show that due to the presence of large thin near-wall turbulent boundary layers populated with small ("attached") eddies whose local size, l, is much less than the boundary layer thickness, δ, that cost exceeds the available computing power by orders of magnitude. As a result, there is no real prospect of using LES in complex engineering computations for a very long time.

On the other hand, the hopes that the conventional RANS turbulence models will soon (if ever) achieve engineering accuracy in the massive three-dimensional separation zones typical for vehicles and airplane components, are rather vague and not supported by the rate of their progress over the last twenty years, even with the benefit of the unsteady solutions (URANS). This pessimism is consistent with the consideration that the dominant, "detached", eddies in massively separated flows are highly geometry-specific which has little to do with the fairly universal eddies typical of the thin shear layers used for RANS turbulence-model calibration. Therefore, LES still is and probably will remain for a rather long time the only defensible tool for a reliable treatment of massive turbulent separation zones.

The recognition of this conflict (non-affordable computational cost of LES in the attached boundary layers and inability of RANS models to provide a reliable prediction of large separation zones) makes it very tempting to create an approach that combines the fine-tuned RANS technology in the attached boundary layers with the "raw power" of LES in the separated regions. In that approach, the "attached", boundary layer, eddies would be modeled, while the larger "detached" ones (populating the separation regions and wakes) would be simulated (small eddies in these regions are also modeled, but have much less influence than the boundary-layer eddies have). Exactly for this reason the approach that claims to reach this goal[1] was given the name Detached-Eddy Simulation.

Though DES is a young technique (only three years have passed since its major idea has been formulated),

*Principal Scientist.

it has already reached some maturity and attracts more and more attention of the aerodynamic community. In the recent review papers of P. Spalart[2,3] major DES features, achievements, and unresolved issues have been discussed in some detail. However the reviews are not restricted to DES, but cover a much wider spectrum of issues of turbulence modeling and simulation. That, inevitably, makes them not quite complete as far as the DES is concerned. Also, some new results, both methodological and applied, were obtained after the reviews have been published. All this justifies an attempt to present a more detailed description of the DES state-of-the-art, as we are undertaking in this paper.

First, in Section 1, we are presenting a general definition of the approach and its specific formulations based on two turbulence models (Spalart-Allmaras or S-A model[4] and Menter or M-SST model[5]). Then, in Section 2, we address some specific numerical issues associated with the demands of the approach. The last, third, section contains some numerical examples that give credibility to the approach.

1. General Description of the DES Technique and its Specific Formulations

The "core" DES idea was expounded in 1997[1] together with its formulation based on the S-A turbulence model. Although, basically, nothing has changed since then, a more thoughtful definition of the technique is now available,[6] not linked with any specific turbulence model. In accordance with this definition, DES is a three-dimensional unsteady numerical solution using a single turbulence model, which functions as a subgrid-scale model in regions where the grid density is fine enough for an LES, and as a RANS model in regions where it is not. The "fine enough" grid for an LES is that one whose maximum (over all three directions) spatial step, Δ, is much smaller than the flow turbulence length-scale, δ_t (this is an integral length scale of the turbulence, much larger than the Kolmogorov scale, of course). Thus in the LES regions little control is left to the model, and the larger, most geometry-sensitive, eddies are directly resolved. As a result, the range of scales in the solution and, therefore, the accuracy of the non-linear interactions available to the largest eddies are expanding when the grid spacing is decreasing. In other words, the model adjusts itself to a lower level of mixing, relative to RANS, in order to unlock the large-scale instabilities of the flow and to let the energy cascade to extend to length scales close to the grid spacing.

In contrast, in the RANS regions (those where Δ is larger than δ_t), the model has full control over the solution, which however remains unsteady and 3D even with a 2D geometry. Note that this situation is typical primarily for thin shear layers (either boundary layers or free mixing layers), which are precisely the flows where the RANS approach is known to be most adequate in terms of computational cost, robustness, and credibility.

An important feature of DES is that the approach is non-zonal and, as such, provides for a single velocity and eddy viscosity field, and there is no issue of smoothness between the RANS and LES regions. Note also that if the boundary layers remain attached and the steady RANS solution is stable, DES finds that solution (unless the grid is refined to the point that the boundary-layer turbulence can be resolved LES-style in all three directions). On the other hand, with grid refinement DES is gradually evolving to the standard LES, and then to DNS.

In general, the user can apply fine resolution only in regions of special interest, which is similar to "tagging" these regions for LES treatment, but is implicit. Another possible way to apply DES is to continue a RANS solution with a highly refined grid in a region of particular interest, for instance, in a landing-gear well or at a rear-view mirror. This will serve if we need fine unsteady physics only there, for example, for a better determination of noise sources.

Now, two specific DES formulations will be presented on the basis of the above background, one using the S-A model and the other the M-SST model.

1.1 S-A Based DES Formulation.[1]

The driving length scale of the RANS S-A model is the distance to the closest wall, d_w. This makes a modification to this model for DES mode quite straightforward (exactly for this reason it was used as a basis of DES in the first publication[1]). The modification consists in substituting for d_w, everywhere in the equations, the new DES length scale, $\tilde{l}$. This length is also based on the grid spacing Δ and is defined as:

$$\tilde{l} = \min(d_w, C_{DES}\Delta), \tag{1}$$

where C_{DES} is the only new adjustable model constant, and Δ is based on the largest dimension of the local grid cell

$$\Delta = \max(\delta_x, \delta_y, \delta_z). \tag{2}$$

Here we assume for simplicity that the grid is structured and that the coordinates (x, y, z) are aligned with the grid cell, but the generalizations are obvious.

For wall-bounded separated flows, the above formulation results in a hybrid model that functions as the standard RANS S-A model inside the whole attached boundary layer, and as its subgrid-scale version in the rest of the flow including the separated regions and near wake. Indeed, in the attached boundary layer, due to the significant grid anisotropy ($\delta_x \approx \delta_z \gg \delta_y$) typical of this flow region, in accordance with (1), $\tilde{l} = d_w$, and the model reduces to the standard S-A RANS model. Otherwise, once a field point is far enough from walls ($d_w > C_{DES}\Delta$), the length scale

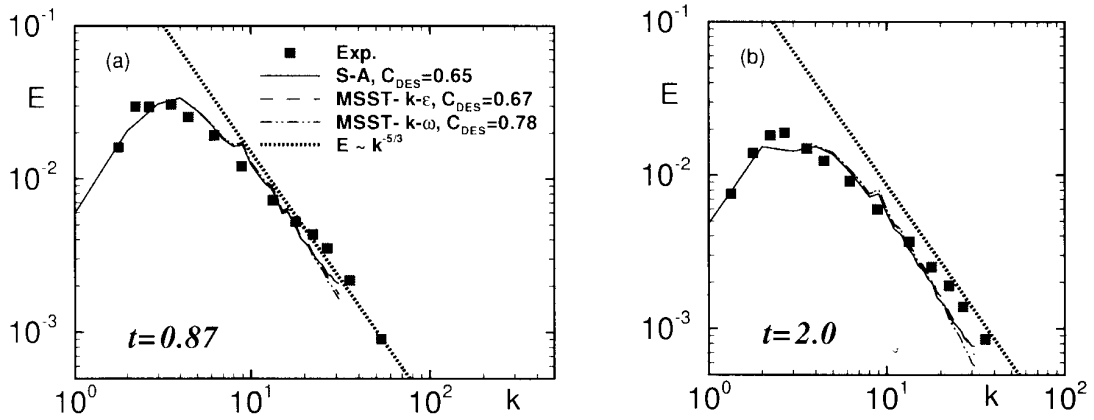

Fig. 1 Spectra in isotropic turbulence: comparison of S-A, and M-SST DES with experiment[9]

of the model becomes grid-dependent, i.e., the model performs as a subgrid-scale version of the S-A model. Note that at "equilibrium" (meaning a balance of production and destruction terms) this model reduces to an algebraic mixing-length Smagorinski-like subgrid model.

1.2 M-SST Based Formulation.

In DES the turbulence is treated by RANS in the attached boundary layer and, maybe, slightly beyond separation. Therefore, the need for accuracy in RANS mode is no less in DES than in pure RANS, and DES versions based on models other than S-A are desirable to provide a range of models for "problem" flows where the S-A model can potentially fail to predict separation accurately enough. Although the DES formulation is immediate only on the basis of the S-A or, say, Secundov's[7] model which also uses a distance to the wall as a turbulence length scale, the DES/S-A link is not fundamental, and other models can be built into DES. Indeed, due to the general DES definition given above, a DES model can be obtained from a RANS model by an appropriate modification of the length scale which is explicitly or implicitly involved in any RANS turbulence model. For now this was done[8] for the k-ω M-SST model, because it is consistently considered as one of the best two-equation RANS models, particularly for separation prediction.

The length scale of the model in terms of k and ω reads

$$l_{k\text{-}\omega} = k^{1/2}/(\beta^*\omega). \tag{3}$$

Now, a non-trivial question arises regarding which specific terms of the model this length scale should be replaced in with the DES length scale

$$\tilde{l} = \min(l_{k\text{-}\omega}, C_{DES}\Delta). \tag{4}$$

This situation is different from that with the S-A model, where there is little freedom of choice. Considering that the role of the subgrid-scale model should not be crucial, our approach was to keep the formulation as simple as possible with the only restriction that at equilibrium the resulting subgrid model should reduce to a Smagorinski-like model. By this we mean that the eddy viscosity is proportional to the magnitude of the strain tensor, and to the square of the grid spacing.

Based on that consideration, the only term of the M-SST RANS model that has been modified to transform it into the DES mode[8] is the dissipative term of the k-transport equation:

$$D^k_{RANS} = \rho\beta^* k\omega = \rho k^{3/2}/l_{k\text{-}\omega}. \tag{5}$$

The modification consists in the simple substitution $\tilde{l}$ (4) for $l_{k\text{-}\omega}$ in (5) which results in

$$D^k_{DES} = \rho k^{3/2}/\tilde{l}. \tag{6}$$

1.3 C_{DES} Calibration.

In order to find the optimal values of C_{DES} and to show that the subgrid-scale versions of the S-A and M-SST models perform fairly well, the models have been exercised in pure LES mode on decaying homogeneous isotropic turbulence, as studied in the experiments of Comte-Bellot and Corsin.[9] The differencing scheme was centered and fourth-order-accurate, and the time integration was by an implicit three-layer second-order-accurate scheme.

The classical M-SST model has two branches, k-ω and k-ϵ. Considering that, we performed separate C_{DES} calibrations for the two branches and then blended the values obtained with the use of Menter's blending function F_1[5]

$$C_{DES} = (1 - F_1)C^{k-\epsilon}_{DES} + F_1 C^{k-\omega}_{DES}. \tag{7}$$

Note that from the standpoint of DES only the k-ϵ branch is important, since precisely this branch is active in the major part of the region where DES functions in LES mode.

Figure 1 shows the spectra at $t = 0.87$ and $t = 2$ in the experiment, computed with the use of the S-A subgrid-scale model at $C_{DES} = 0.65$ and with the M-SST one at $C_{DES}^{k-\epsilon} = 0.61$ and $C_{DES}^{k-\omega} = 0.78$. As seen in the figure, with those constants, the agreement with the experiment is fairly good, and the spectral slopes are close to $-5/3$ near the cutoff wave-number. Also, the energy decay has been about 75% which is close to the experiment, and the average eddy viscosity scales closely with $\Delta^{4/3}$ as expected in the inertial range. The test seems to be quite satisfactory and gives credibility to the subgrid-scale versions of the S-A and M-SST models and the C_{DES} values. These values appear optimal for the differencing scheme used; schemes with more numerical dissipation may couple best with somewhat lower values.

2. Numerical Issues

As far as the author is aware, all the DES applications published till now were performed with the use of implicit upwind schemes. For instance, for the incompressible flows,[6,10,11] the time accurate (with dual time stepping) implicit upwind-biased scheme of Rogers and Kwak[12] is used (the scheme is of fifth order in space and of second order in time). In the only available example of DES of compressible flow,[13] the computations are performed with the use of the unstructured Cobalt code which is upwind and of second order accuracy both in space and time.

The choice of implicit upwind schemes for full DES (as opposed to the homogeneous turbulence "box") was dictated by the hybrid nature of DES and, in particular, by the lack of stability of the less-dissipative centered schemes in the flow regions where DES is operating in the RANS mode. The causes are well known. They are: high values of the cell Reynolds number (even based on the eddy viscosity), dispersion (especially at angles to the grid lines), non-uniform grid spacing and coefficients, nonlinearity. On the other hand, in the LES regions of DES the upwind schemes seem to be sub-optimal since they are commonly considered as "too dissipative" for LES (e.g., Ref.14). Thus, though a statement such as "upwind schemes are unacceptable for LES" cannot be correct (any numerical method, if consistent, results in an acceptable accuracy with a grid fine enough), this issue of numerical dissipation in DES does exist, and requires attention. Excessive dissipation does not result in an unstable or meaningless solution, but it prevents the solution from taking full advantage of the grid provided. It stops the energy cascade before the SGS eddy viscosity does, or in collaboration with the eddy viscosity but still at scales that are larger than the best possible.

An approach that allows to resolve it or, at least, to weaken significantly the harm caused by upwinding in the LES regions of DES is suggested in Ref.8. It is based again on the hybrid DES nature and uses the following hybrid central/upwind approximation of the inviscid fluxes, F_{inv}, in the governing equations:

$$F_{inv} = (1 - \sigma)F_{ctr} + \sigma F_{upw}, \tag{8}$$

where F_{ctr} and F_{upw} denote respectively the central (fourth order) and upwind (third/fifth order) approximations of F and σ is a blending function. It is designed so that in the regions treated in the RANS mode, σ is close to its maximum value $\sigma_{max} = 1.0$, resulting in an "almost upwind" scheme, while in the LES regions σ is close to zero resulting in an "almost centered" scheme. In addition, the blending function has to ensure the choice of the upwind scheme in the irrotational region of the flow. This is needed to guarantee stability of the scheme with the coarse grids typically used in such regions. A specific form of the blending function[8] is as follows:

$$\sigma = \sigma_{max} \tanh(A^{C_{H1}}). \tag{9}$$

Here the function A is defined as

$$A = C_{H2} \max\left\{\left[(C_{DES}\Delta/l_{turb})/g - 0.5\right], 0\right\}, \tag{10}$$

the turbulence length scale, l_{turb} is defined via the eddy viscosity and a combination of the magnitudes of the mean strain, S, and vorticity, Ω,

$$l_{turb} = (\nu_t + \nu)/[C_\mu^{3/2} K]^{1/2}, \tag{11}$$

where $K = \max\left\{[(S^2 + \Omega^2)/2]^{1/2}, 0.1\tau^{-1}\right\}$, τ is the characteristic convective time, and the parameter g is introduced to ensure the dominance of the upwind scheme in the disturbed irrotational flow regions where $\Omega \ll 1$ and $S > 0$:

$$g = \tanh B^4,$$

$$B = C_{H3}\Omega \max(S, \Omega)/\max[(S^2 + \Omega^2)/2, 10^{-20}]. \tag{12}$$

The constants of the blending functions are: $\sigma_{max} = 1.0$, $C_{H1} = 3.0$, $C_{H2} = 1.0$, $C_{H3} = 2.0$.

In Fig.2 a snapshot of the blending function σ is presented from our DES of a circular cylinder[8] (see Section 3.2 below) together with a simultaneous snapshot of the eddy viscosity. It gives a clear idea of the performance of the suggested approximation. In the vortical area of the cylinder wake, where DES performs in LES mode, σ is close to zero and the scheme is virtually the centered fourth-order one. Conversely, in the near-wall RANS regions and, also, in the irrotational outer part of the flow, σ is close to 1.0 and the scheme is effectively the fifth-order upwind one.

Included in the following examples of DES performance with the pure upwind scheme, are some examples that illustrate the capabilities of the hybrid scheme in more detail.

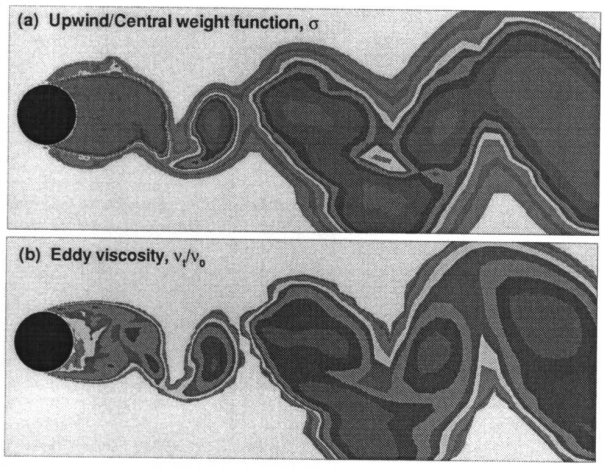

Fig. 2 Simultaneous snapshots of blending function σ (see eqn.(9)) and eddy viscosity from DES of circular cylinder at $Re = 50,000$

3. Computational Examples

In this section we are presenting numerical examples supporting the credibility of DES and outlining the areas requiring effort. The examples are restricted to our own work, but the literature includes other flows (a sphere,[10] a missile base,[13] and a channel flow[15]), and at least six separate groups are known to be pursuing DES.

3.1 NACA 0012 Airfoil at high angle of attack.

This was the first true, 3D, application of DES and, due to its very promising results, it had a decisive influence on the further DES development and applications. Though in Ref.11 the computations were performed with the use of the S-A based DES (1)–(2), below we present also some results obtained later[8] with the use of the M-SST DES (4)–(6).

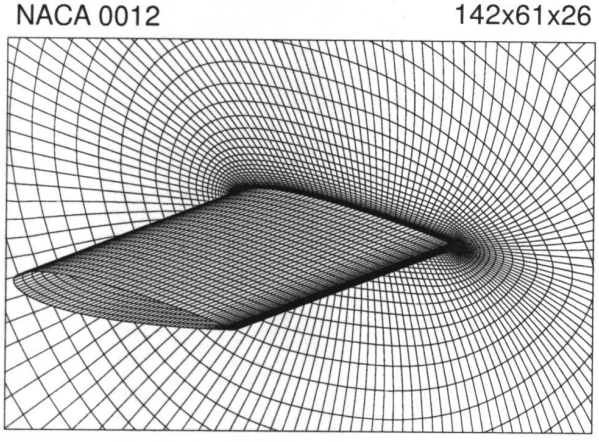

Fig. 3 Fragment of the computational O-grid used in DES of NACA 0012 airfoil

The Reynolds number based on the airfoil chord c in the simulations was equal to 10^5, and the angle of attack was varying from 0 to 90 degrees. In order to avoid arbitrarily adjusting transition points, the model was used in fully-turbulent mode (the free-stream value of the eddy viscosity ν_t was set equal to the molecular viscosity, which puts the working variable $\tilde{\nu}$ outside the basin of attraction of the zero value). The computational-domain size in the xy-plane was equal to $15c$, and the spanwise period was $1 \times c$. The grid used in the computations was of the O-type in xy-planes (see a fragment in Fig. 3), with a uniform spanwise step δ_z equal to $(1/24)c$, resulting in a total number of nodes $141 \times 61 \times 26$, which is certainly "modest" by LES standards for this high a Reynolds number. The near-wall grid spacing was $10^{-4}c$, following normal practice for RANS at $Re = 10^5$. The time step was $0.025c/U_\infty$ and for a complete separated case (100–200 chords of travel) the cpu time was 4–8 weeks on a Pentium II/266MHz computer with the use of the Rogers and Kwak scheme.[12]

First, in order to support the claim that DES automatically finds a 2D steady solution for the fully attached flows, simulations were performed below the stall angle. It turned out that the DES solution indeed is 2D and steady and is virtually identical to the 2D RANS solution obtained with the standard S-A model.

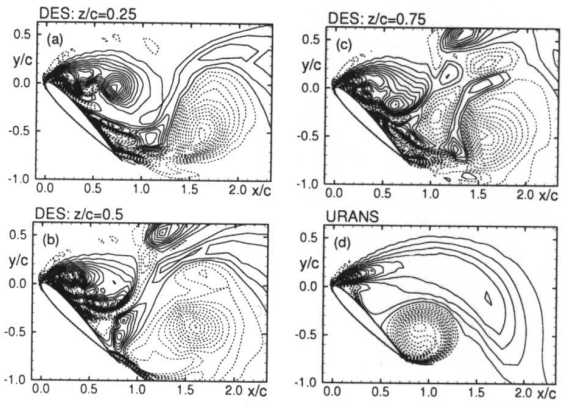

Fig. 4 Side-views of the spanwise vorticity at different cross-sections of the DES (a)-(c) and the URANS 2D solution (d) for NACA 0012 airfoil at $\alpha = 45^o$ and $Re = 100,000$.

For the régimes beyond stall with massive separation, the situation is quite different. Figure 4a-c shows snapshots of the spanwise vorticity at three simultaneous cross-sections of the DES at $\alpha = 45°$. Eddies with sizes rather smaller than c are resolved near the upper airfoil surface, although not very fine with this grid and numerical scheme. In contrast to that, URANS, meaning an unsteady 2D computation with the standard S-A RANS model, suppresses the smaller eddies and sheds large smooth vortices as shown in Fig.4d, which resembles other URANS studies (e.g., Refs.16, 17). The three DES frames are noticeably different, indicating that the simulation has sustained the ran-

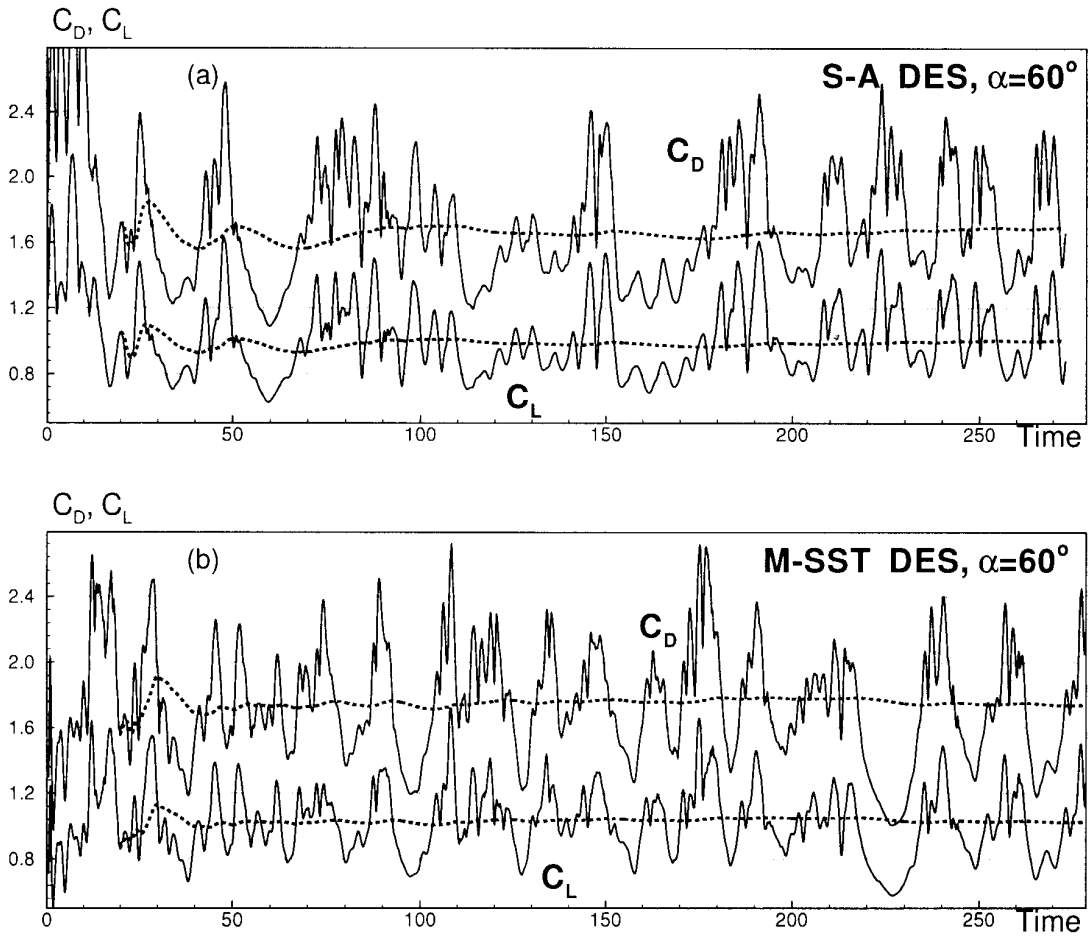

Fig. 5 Time-dependent (solid lines) and time-averaged (dashed lines) drag and lift forces on the NACA 0012 airfoil at $\alpha = 60°$: comparison of the S-A and M-SST DES predictions (20 initial time units are not used for averaging)

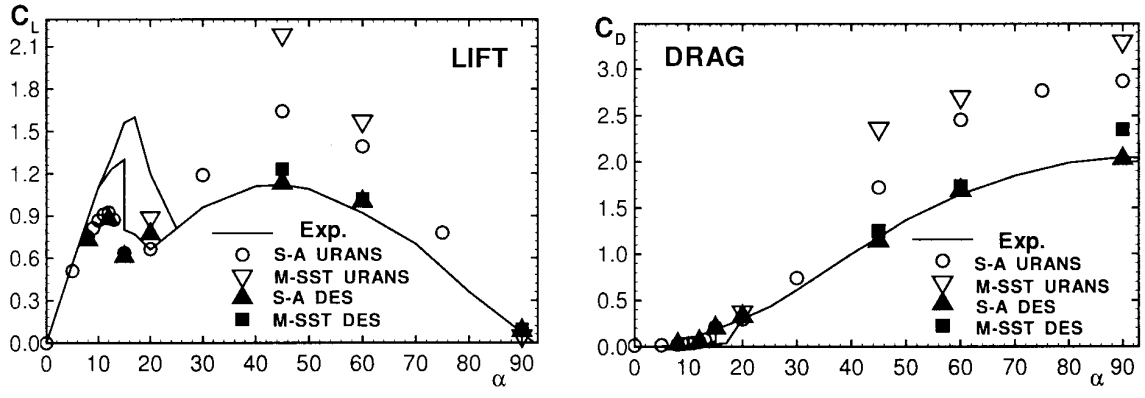

Fig. 6 Lift and drag coefficients of the NACA 0012 airfoil: comparison of DES and URANS predictions with the experimental data[18–21]

dom initial three-dimensionality. Note that, unlike DES, 3D URANS of this flow damps out the three-dimensionality (unless it has a very long spanwise length scale) and results in a 2D solution.

Quite similar results are obtained with the use of the M-SST DES, and we did not detect qualitative or significant quantitative differences in the resolved flow structures between the two models.

Figure 5 shows the time-dependent lift and drag coefficients for the 60° case from the simulations with the S-A and M-SST models. In contrast with the strictly periodic behavior typical of URANS, DES displays some chaotic features. Though physically correct, this behavior means rather long time samples are needed for reliable averaged forces, which is unfortunate in terms of computational cost. Figure 6 presents the averaged forces over a wide range of angle of attack and compares DES predictions with those of URANS and with the experimental data[18–20] below stall and[21] above the stall angle. Two curves in the plot are crudely showing the experimental scatter, in the 13° to 25° range for $Re_c = 10^6$ (at the angles higher than 25° we have only one source and are unable to estimate scatter). The post-stall measurements are at $Re_c = 2 \cdot 10^6$, while our DES is at only 10^5. This helps contain computational cost and considering the weak Reynolds-number dependence after stall, has a small impact on the flow.

At angles of attack below stall the agreement with the data is not perfect, which is not surprising considering the sensitivity of the attached flow to the Reynolds number and transition. For $Re_c = 10^5$ with natural transition, experiments suggest a value of the maximum lift coefficient C_{lmax} in the 0.8 to 0.95 range,[19] while the fully-turbulent simulations return a C_{lmax} near 1.0 at α near 13°.

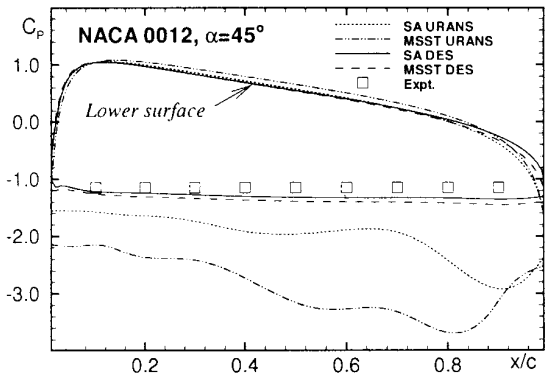

Fig. 7 Pressure coefficient distribution over NACA 0012 airfoil: comparison of DES and URANS predictions with the experimental data for a normal flat plate[23]

Beyond stall, the agreement between DES and experiment for both integral forces (Fig.6) and pressure coefficient distribution (Fig.7) is gratifying. This is consistent with results of Najjar and Vanka,[22] who performed 3D DNS of a normal flat plate at $Re_c = 10^3$. Also in the line with their findings, at high angles of attack (over 30°) 2D URANS suffers from a very large drag and lift excess (Fig.6) and the C_p on the upper surface of the airfoil is far from uniform (Fig.7). Finally, though some disparity between the two DES models does exist, it is much less than that between the same two models in URANS mode.

Based on this first application, DES appeared highly promising which made it worthwhile to explore its capabilities as applied to other flows.

3.2 Circular Cylinder.

This flow is an obvious test for an approach with claims over separated flows. As M.Breuer puts it in his recent paper on the cylinder LES,[24] "... successful applications for this test case can be considered as the ticket to the real world applications of LES". Therefore, DES success for this flow would give the approach a deeper credibility than the thin airfoil considered above. In the latter, both LES and RANS capabilities of DES are exercised, but not truly in the same solution. A pure RANS method would give the same results as DES at low angles of attack, the flow being attached. On the other hand, a pure LES method could be manageable and might give fair results at high angles of attack, when the major features of the flow have little sensitivity to the boundary layer turbulence (which an LES of the whole domain could not resolve with present computers). Another point of great interest and some concern in DES is the "grey area" between RANS and LES regions. With DES, at separation, the shear layer has no "LES content" (i.e., 3D unsteady eddies the size of the boundary-layer thickness). So DES seems to be most justified if a rapid new instability, of large scale, overwhelms the turbulence inherited from the boundary layer (if any). This is more likely if the separation is from a sharp edge or at least a thin one, as on the airfoil. The cylinder is less forgiving, and so provides a better opportunity for "grey area failure". Finally the cylinder is known for its drag crisis, which reflects the great differences in separation between laminar and turbulent boundary layers. The challenges in DES associated with that principle feature of the flow are not trivial. For Laminar Separation (LS), the model needs to be dormant in the laminar region, and arise in a spontaneous manner after separation, which can be delicate. A Trip-Less (TL) approach permitting to resolve this issue[16,25] has been tested only in 2D RANS which does not automatically guarantee its feasibility in DES. Finally, cases with Turbulent Separation (TS) are wholly out of reach of whole-domain LES. In DES, they give the model in RANS mode control over separation and so stress its accuracy in this mode. Thus the cylin-

der taken over LS and TS regimes represents a much more severe and substantial test case for DES, giving the opportunity to show that it is competitive with both RANS and LES. Since the results obtained in the course of this study are presented and discussed in detail in Ref.6, here, we are focusing only on the major findings of Ref.6 and on some recent, not yet published, results.

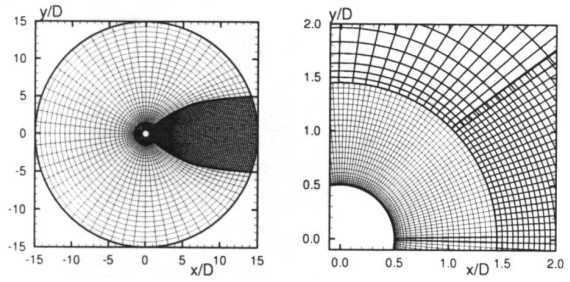

Fig. 8 Medium computational grid used for DES of circular cylinder. Inner block 150×36**, wake block** 74×36**, outer block** 59×30

A typical ("medium") grid used in the simulation is shown in Fig.8. It has three blocks (total size about 500,000 nodes) with a coarser spacing in the irrotational region, relative to the near-wall and wake regions and is designed so that in the region near (x, y)=(0.75, 0.5) where there is high activity and the solution is clearly of LES type, the cells of the grid are close to a square with the side Δ. The spanwise period is equal to $2D$ (D is the cylinder diameter) and the 3D grids are balanced, in the sense that δ_z is close to Δ also. A grid refinement study has been performed with three successive grids with Δ ratio $\sqrt{2}$.

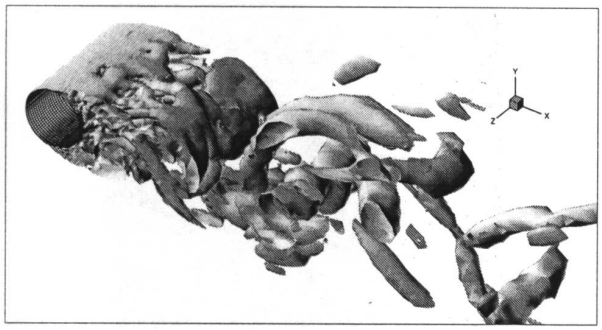

Fig. 9 Visualization of the LS circular cylinder flow at $Re = 50,000$ **(surface** λ **=1)**

In Fig.9 we show the visualization of the LS flow at $Re = 5 \cdot 10^4$ on the medium grid. It is meant to build confidence in the three-dimensional character of the solution, and the spanwise domain size. We use the imaginary part, λ_i, of the complex conjugate eigenvalues of the velocity gradient tensor[26] to bring out vortices. The figure reveals the dominant 2D von Kármán vortex-shedding mode, but also intense streamwise vortices transverse to the Kármán street. It is very consistent with DNS and LES studies of similar flows. This figure reflects how DES functions in the attached boundary layers, whether laminar or turbulent: the resolved solution is smooth with weak variations in z and t. In TS cases the boundary layer turbulence is fully modeled, the model provides all the Reynolds stress, and even its large eddies are not represented.

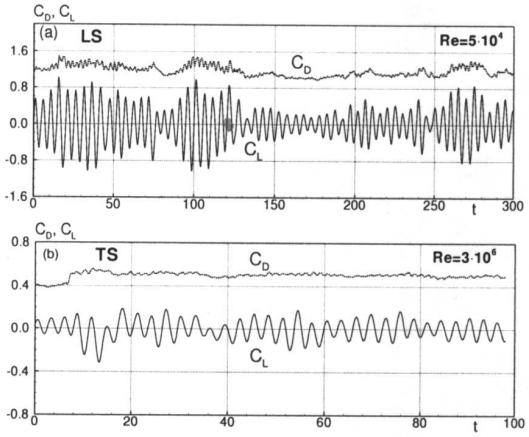

Fig. 10 Time-dependent lift (solid lines) and drag (dashed lines) coefficients from S-A DES of circular cylinder; (a)–LS flow; (b)– TS flow

Figure 10a illustrates the strong chaotic modulations of the shedding phenomenon for the LS flow regimes. The time scale of the modulations is of the order of 10 times the von Kármán shedding period. Again, this is very consistent with DNS for the flat plate at 90°,[27] LES of circular and square cylinders[28,29] and experiments.[30–32] This behavior suggests that any fine comparisons between drag coefficients, for instance, are drastically limited by this feature, and that any simulation studies of bluff bodies with LS that used only a few shedding cycles should be seriously reconsidered. For the TS regimes this effect, though again present, is a good deal weaker (see Fig.10b) which makes them less "time-sample sensitive".

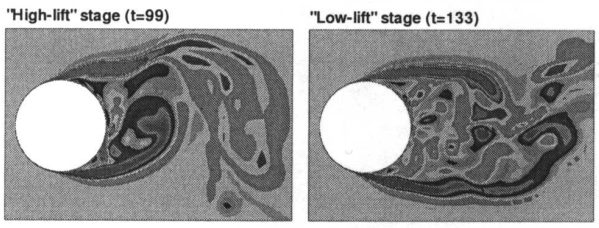

Fig. 11 Comparison of spanwise-vorticity snapshots at the stages of "high"($t = 99$**) and "low"(**$t = 133$**) lift oscillations (see Fig.10a)**

Figure 11 reveals a striking visual difference between a time of high and low lift oscillations for the LS flow. These two frames are from one simulation at two differ-

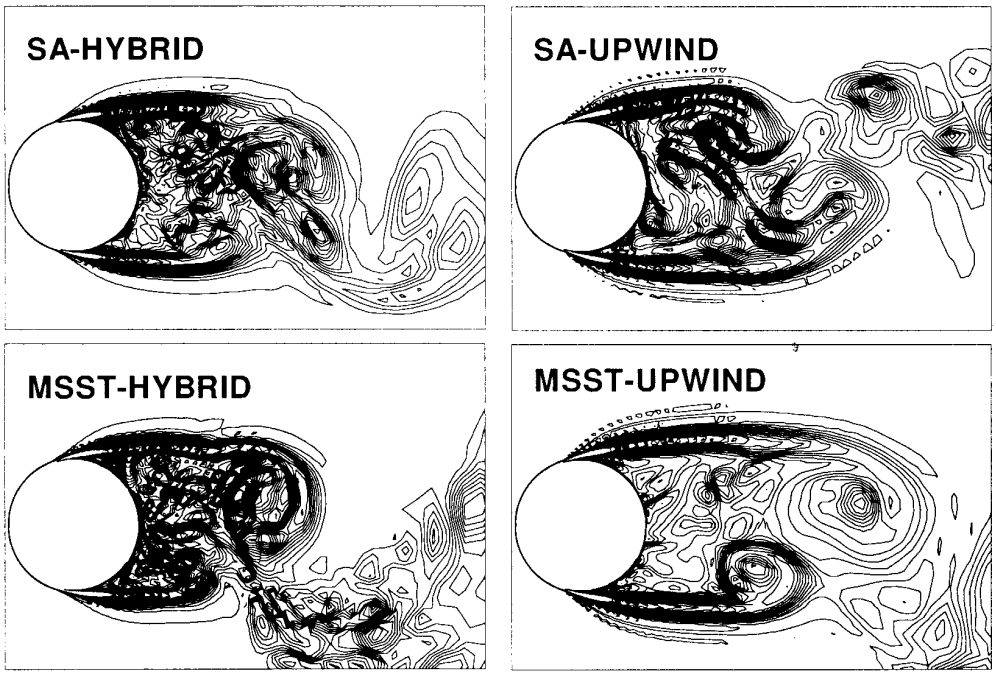

Fig. 12 Effect of the turbulence model and numerical method on DES of a cylinder: spanwise-vorticity contours in a plane of LS flow at $Re = 50,000$

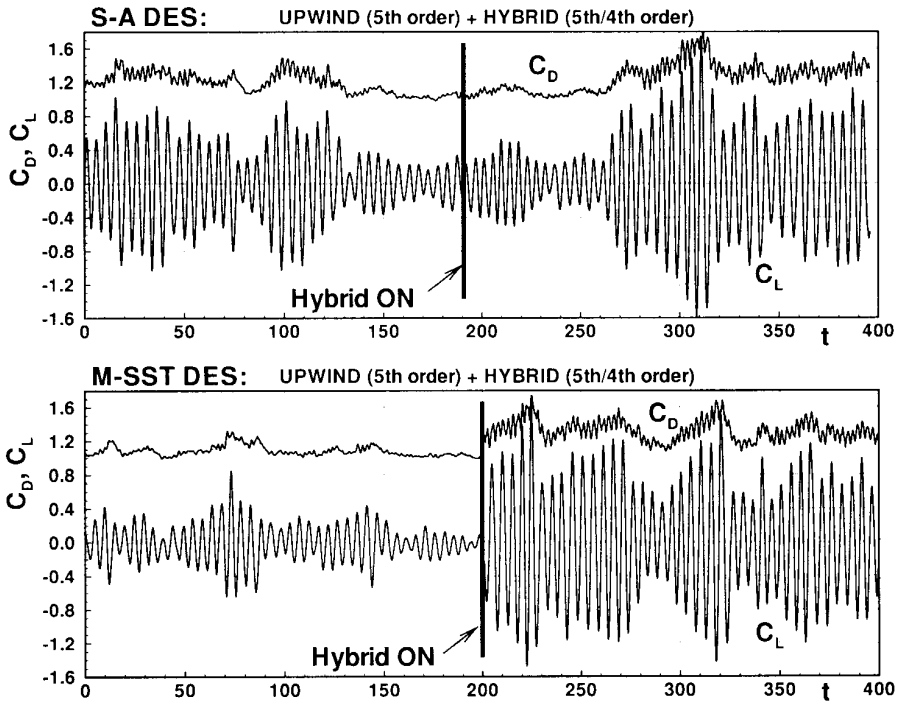

Fig. 13 Effect of the turbulence model and numerical method on DES of a cylinder: time dependent lift and drag of LS flow at $Re = 50,000$

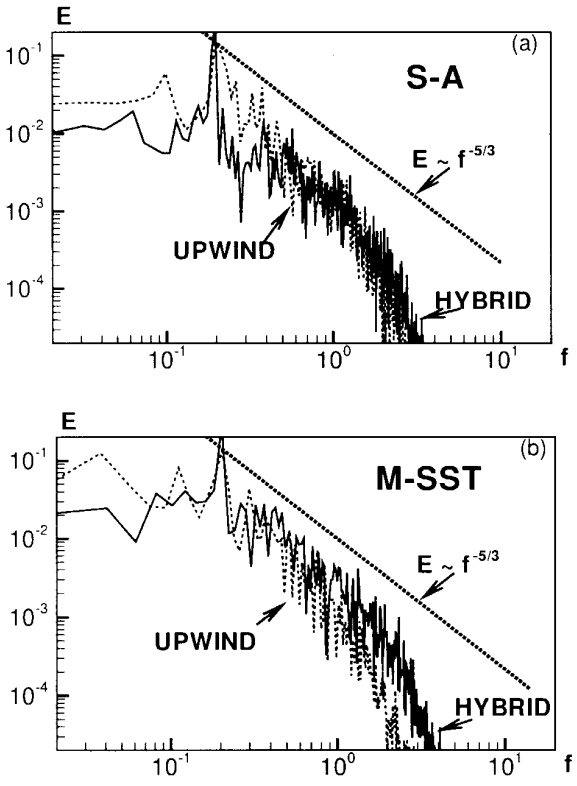

Fig. 14 Effect of the turbulence model and numerical method on DES of a cylinder: resolved energy spectra of LS flow at Re=50,000

ent moments, both late enough to be ostensibly mature ($t = 99$ and $t = 133$). Yet, at first sight it looks like they have different grids or turbulence models. The change in the flow pattern is quite similar to that described in Ref.27 for DNS of the normal flat plate.

Figures 12–15 give an idea about the effects of numerical scheme and turbulence model on DES solutions. In particular, Fig.12 shows spanwise-vorticity snapshots computed on the medium grid for the LS flow at $Re = 5 \cdot 10^4$ using the fifth-order upwind and the hybrid (fifth order upwind/fourth order centered) schemes, and the S-A and M-SST models. As expected, with the hybrid scheme, the solution displays smaller vortices with both models. However, with the M-SST model the effect of the scheme is much more visual. The same trends are even more striking in the time-dependent forces shown in Fig.13, and are observed also in Figs.14-15, where we present the spectra of the resolved kinetic energy at the wake centerline (at $x = 1D$), and the resolved and modeled shear stresses respectively. The resolved Reynolds stresses are produced by averaging the flow field that was calculated, while the modeled stresses are the average of the stresses created by the eddy viscosity.[15]

Figure 16 compares experimental distributions[30] of the pressure coefficient for the flow with LS with those

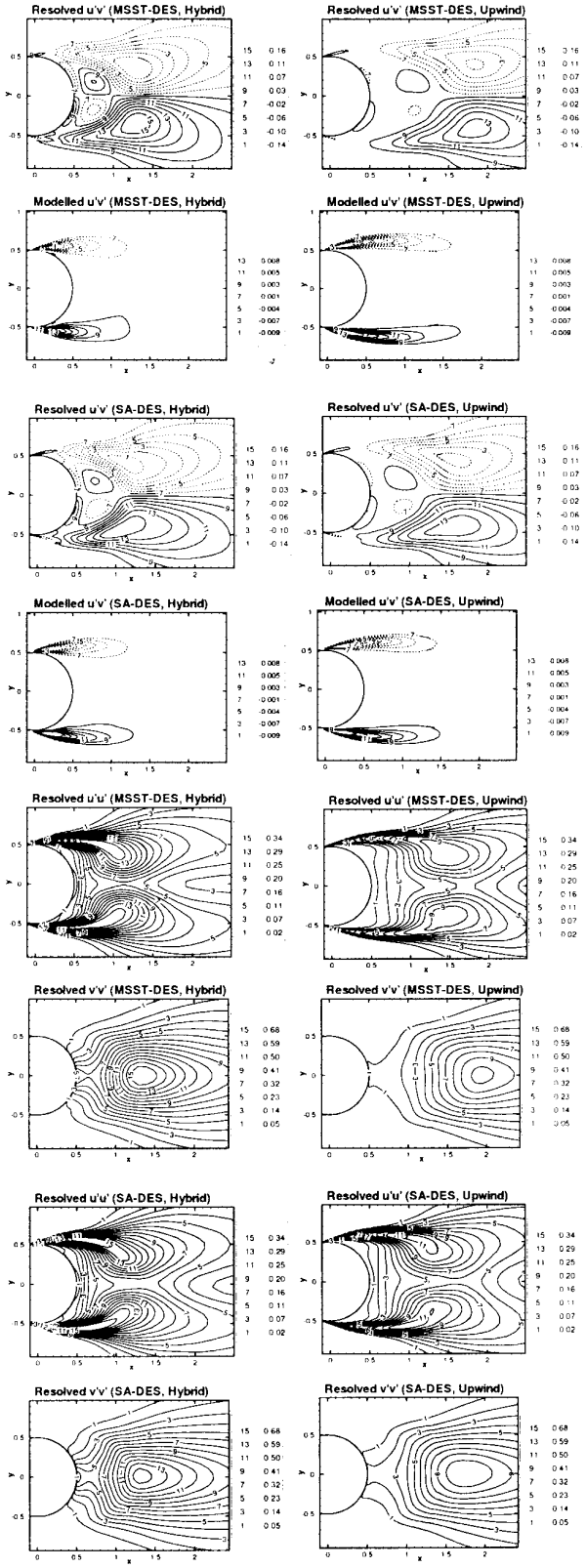

Fig. 15 Effect of the turbulence model and numerical method on DES of a cylinder: resolved and modeled stresses of LS flow at $Re = 50,000$

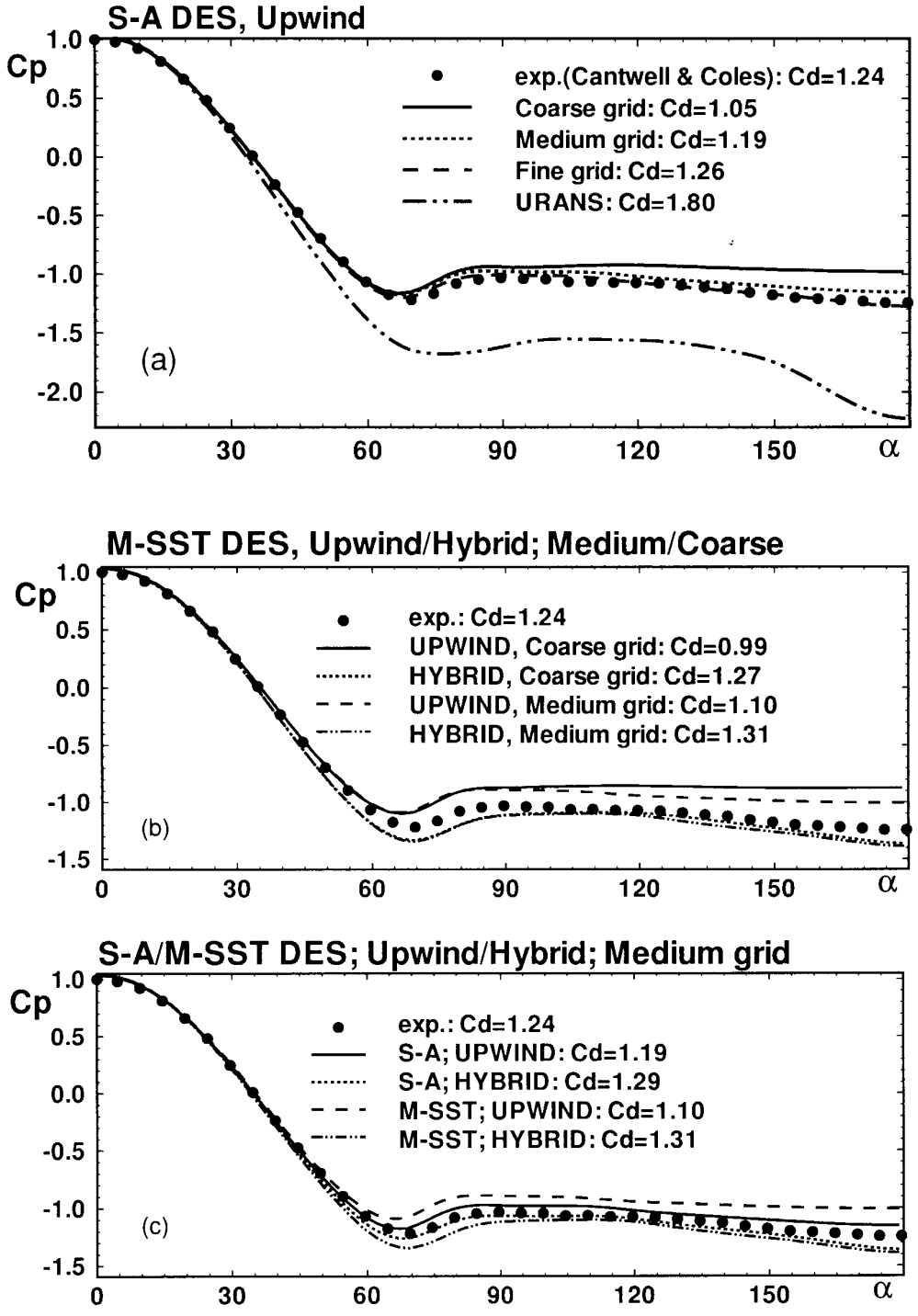

Fig. 16 Effect of grid size, turbulence model and numerical method on the pressure distribution over a cylinder: pressure coefficient of LS flow at $Re = 50,000$

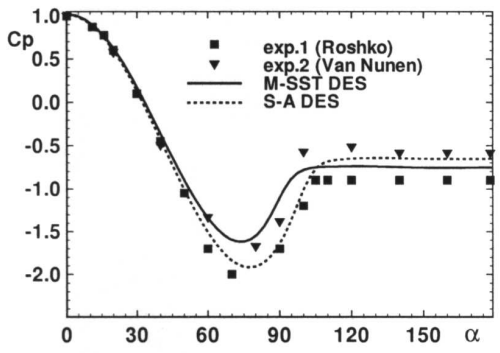

Fig. 17 Effect of the turbulence model on the pressure coefficient distribution over a cylinder: TS flow at $Re = 50,000$

from DES performed with the two models and two numerical schemes. The upper frame of the figure demonstrates an impressive agreement with experiment and strongly suggests grid convergence with the fifth order upwind scheme. Note that such convergence has been elusive in LES of this flow. Also, just as for the airfoil, 2D URANS gives vortex shedding at the correct frequency, but the shedding is much too regular,[16] and the drag is much too high. The other frames of Fig.16 show coarse- and medium-grid results with both numerical schemes and turbulence models. It can be concluded that the effect of the model is comparable with numerical inaccuracies caused by a coarse grid or excessively dissipative numerics, which seems to be quite consistent with the premise of LES.

We expected a stronger model-dependence for the TS flow regimes, in which the RANS mode of DES is responsible for prediction of turbulent separation, and so the M-SST model might be expected to perform better than the S-A one. However, as seen in Fig.17, due to quite a noticeable scatter in the experimental data for this flow regime,[33,34] it is difficult to give a definite preference to either of the two models.

3.3 Other Examples.

In this section we are presenting additional examples of our DES studies. They are not as complete as that of the circular cylinder flow, but showing them still seems to be meaningful and to give a much wider idea about the range of DES potential applications and capabilities.

3.3.1 Backward-facing-Step (BFS) of Jovic and Driver at $Re_h = 5000$.[35]

This flow is a very appreciated test case for evaluating the capability of RANS turbulence models to capture the major features of a flow with separation and reattachment. The test however confronts the DES user with a crucial decision. In one approach, the incoming turbulent boundary layer has "DES content" or, in other words, its turbulence is resolved. Then we have an LES over the whole domain, much like we did in a channel.[15] In the opposite approach, we assume that the incoming boundary layer is thin enough relative to the step height h that the recirculating bubble is dominated by eddies much larger than the incoming eddies, so that it is not essential to resolve those. Then the incoming boundary layer is treated by RANS; this is controlled by the grid spacing in the usual fashion. This second approach is much closer to the reality of DES in aerodynamic flows, and was adopted. Note that some of the RANS models, including S-A and, especially, M-SST models have been shown be quite accurate for this specific flow.[36] This is probably due to the thin-shear-layer character of the flow. Therefore, DES is competing with a rather successful technology.

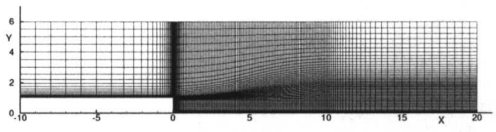

Fig. 18 Computational grid used for DES of BFS flow.[35]

The computational domain in our DES of this flow consists of an entry section of length $10h$ prior to the step and a $20h$ postexpansion section, while the spanwise dimension is $2h$, with periodic boundary conditions. The simulation uses $181 \times 76 \times 22$ grid points in the streamwise, wall-normal, and spanwise direction respectively. The spanwise grid-spacing is uniform ($\delta_z = 0.1$), and the grid in the xy-plane is shown in Fig.18. In the near-wall region the grid spacing is the same as that in our RANS computations of the same flow.[36] It ensures a maximum near-wall step in wall units not higher than 0.4 and, according to the grid-sensitivity study performed for RANS,[36] is quite sufficient to obtain a virtually grid-independent solution. In the LES region, just as in the circular cylinder simulations, the grid cells are close to cubic.

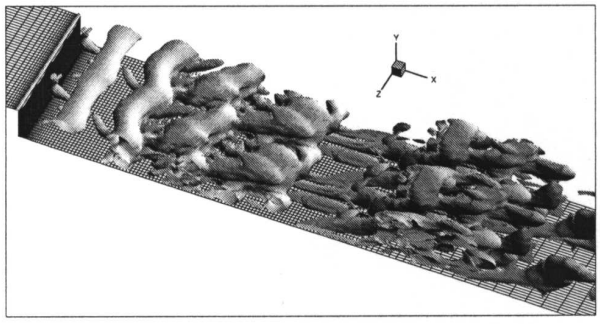

Fig. 19 Visualization of the BFS flow (surface λ=0.25).

Figure 19 shows the flow visualization from the M-SST DES by means of the "swirl" surface $\lambda = 0.25$.

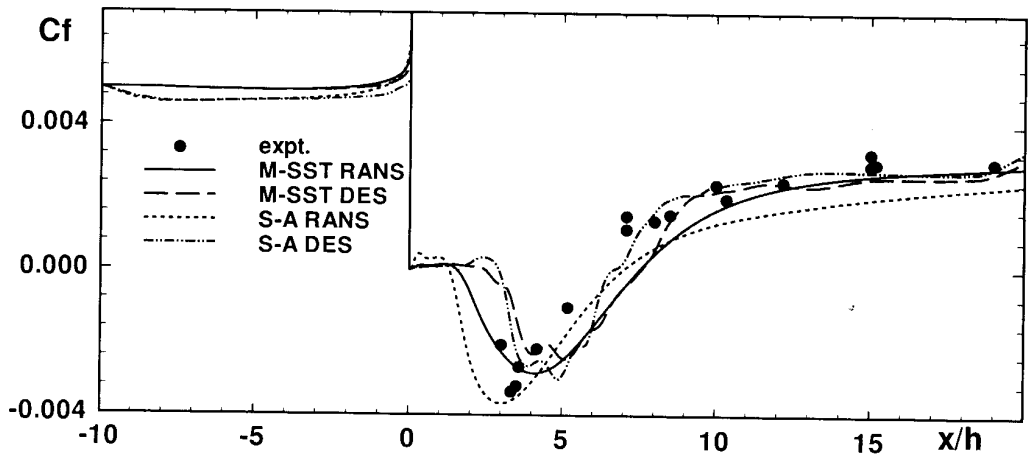

Fig. 20 Comparison of DES and RANS predictions of friction coefficient distribution over the BFS with the experiment.[35]

It reveals all the typical flow structures observed in DNS and LES of the BFS flow (e.g., Refs.37–39), namely, the quasi-two-dimensional Kelvin-Hemholtz rolls convected downstream and then pairing, the streamwise vortices forming farther downstream, and gradual transformation of the flow to an essentially 3D one. Thus, in spite of the rudimentary treatment of the inlet region mentioned above, DES is still capable of reflecting the major 3D unsteady physics of the BFS flow discussed in detail in the literature.

As far as the mean flow is concerned, the accuracy of DES turns out no worse than that of the corresponding RANS; it is also much less model-dependent. This is seen in Fig.20, where we compare time- and span-averaged C_f distributions from the S-A and M-SST DES with the corresponding steady RANS distributions. Note also that in the region of flow recovery after reattachment, generally the most challenging for RANS, DES with both models performs tangibly better than even M-SST in RANS mode. Therefore, the strength of LES appears to be showing even in this flow region, which is two-dimensional and near-parallel in the mean.

3.3.2. Triangular cylinder in a plane channel.[42]

This flow has been used as a benchmark in many numerical studies (e.g., Refs.17, 40, 41) performed both with the use of steady and unsteady RANS, and to this date may have presented the most impressive example of the superiority of URANS.[17]

The grid used in our S-A DES of this flow had two blocks with 93 × 89 and 137 × 61 nodes in xy-plane (see Fig.21). The span period in DES was equal to $1a$ (a is the triangle side), and the grid spacing in the z-direction $\delta_z = 0.05$ which results in a total number of grid points equal to 366,000. S-A URANS computations were performed on the same grid as that used for DES.

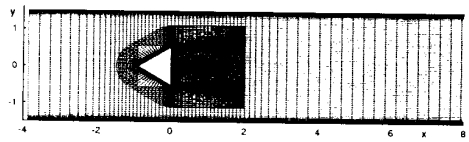

Fig. 21 Computational grid used for DES of a triangular cylinder in a plane channel.[42]

Figure 22 compares spanwise-vorticity snapshots from DES at different xy-planes with one from the 2D URANS. The picture is quite consistent with what we observe in all the other cases. Again, just as for other massively separated flows, URANS predicts regular von Kármán vortex-shedding, while DES reveals much more small-scale activity and three-dimensionality. However, possibly due to the geometrical restrictions caused by the channel walls, the amplitudes of the oscillations and the widths of the wake in URANS and DES are not as different as, for example, for the circular cylinder in "free air" considered above. As a result, the time-averaged forces and other mean-flow characteristics computed on the basis of URANS and DES are not highly different. This is seen in Fig.23, where we compare S-A URANS and DES streamwise mean velocity distributions along the wake centerline with the experimental data.[42] Still, DES agrees somewhat better with the data than URANS, especially in terms of the length of the recirculation zone, and is virtually as good as the URANS of Refs.17, 40, which are the best found in the literature for this flow.

3.3.3. Raised airport runway.

The runway is a new extension to that of the Santa Catarina Airport (Funchal, Madeira Island, Portugal). It is built on stilts, 185 m wide and 58 m high, on the

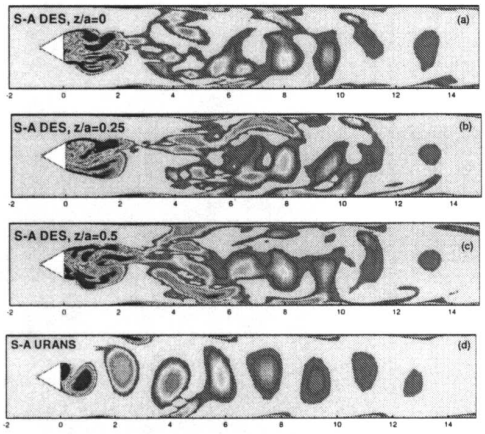

Fig. 22 Side-views of the spanwise vorticity at different cross-section of DES (a)–(c) and URANS 2D solution (d) for triangular cylinder.

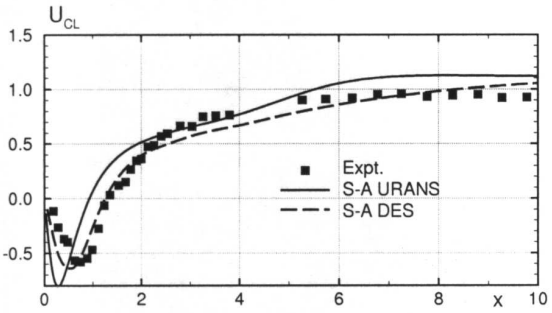

Fig. 23 Comparison of DES and URANS predictions of the streamwise velocity distribution along the triangle wake centerline with the experimental data.[42]

island-side. This rare configuration, in case of cross-wind from the ocean, is likely to cause separation off the edge of the runway platform, creating lateral wind shear at some height over the runway and reversed flow at its surface, as well as high relative turbulence intensity. The objective of the simulation was to quantify these effects.

A schematic of the domain with a three-block computational grid in xy-planes (the total number of grid nodes in one plane is about 34,000) used for DES of the cross-wind-induced flow in the vicinity of the runway is shown in Fig.24. We took the shape of the hill at one station along the runway. Shape details with lengths up to about 2 m near the platform edge are omitted. The "spanwise" period (really, the period in the runway direction) is set equal to 1/3 of the platform width (on the basis of our experience with the NACA 0012 airfoil, this seems to be sufficient to capture the major 3D structures at moderate angles of attack). In the z-direction, the grid has 22 uniformly spaced planes resulting in about 750,000 nodes.

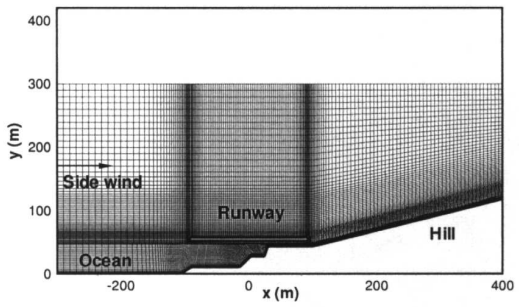

Fig. 24 Computational grid used for DES of raised runway in cross-wind.

The inflow condition at the left boundary is a uniform velocity with a thin boundary layer at the ocean surface. This ignores the true thickness of the atmospheric boundary layer, which is of the order of 1000m, or five times the runway width. The ideal DES would include that profile, including the Ekman skewing, as well as LES content, since the length scale of these eddies is large. However, the peak velocity excursions in such a boundary layer are roughly 15% of the wind velocity, which is fairly small compared with the excursions generated by the separated shear layer, as we show below. Therefore, the strongest effects of the wind are captured.

The Reynolds number based on the wind velocity and the runway width is high: $1.2 \cdot 10^7$. Therefore the results presented below, normalized by the wind velocity value, can be considered as insensitive to any further Reynolds-number increases.

The turbulence model was the S-A one with a wall roughness correction,[3] and the surfaces of the ocean and hill were considered as rough with a uniform conventional roughness of 1 m height. Roughness changes would have more effect than Reynolds-number changes. Note that Equation (6) in that paper contains an error, χ in the denominator should be replaced with $\widetilde{\nu}/\nu$.

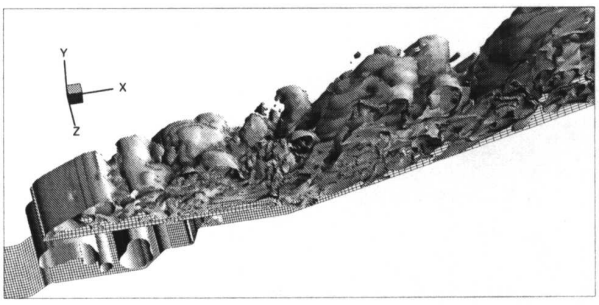

Fig. 25 Visualization of the raised runway flow (surface λ=0.25).

Figure 25 is a flow visualization by a typical swirl iso-surface (λ =0.25). As might be expected considering the specific terrain relief and the narrowness of the

"gap" between the runway and the hill, which forces the flow over the platform, it reveals separation of the flow off the edge of that runway platform, shear layer roll-up, and formation of essentially 3D roller/rib structures, as is typical for thin bodies at high angles of attack. Therefore the simulation fully confirms the expectation that the flow above the runway would be massively separated, essentially 3D, and unsteady.

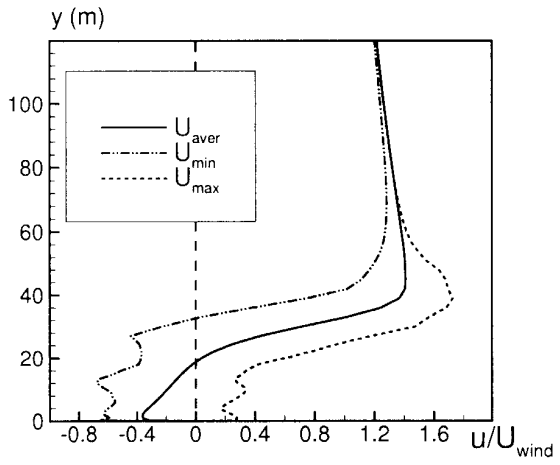

Fig. 26 Vertical profiles of the averaged, minimum, and maximum wind velocity at the middle of the runway.

In order to assess the runway flow conditions quantitatively, the minima and maxima of the x-velocity component were collected over time and over the spanwise domain. The profiles of the quantities $u_{max}(y)$ and $u_{min}(y)$ above the runway centerline are plotted in Fig.26 together with the time/span averaged velocity, $u_{aver}(y)$. A striking feature of the figure is that the range of the velocity variations (the strength of the "wind gusts") is about $\pm 100\%$ of its nominal value.

We found that for the same problem setup, the URANS solution turns out to be strictly steady. Therefore, though the span- and time-averaged DES velocity field is fairly close to that steady solution (see Fig.27), URANS does not allow any of the unsteady content which is crucial considering the purpose of the study. Thus, the results show that applying URANS instead of DES to evaluate the proper wind limits for take-offs/landings at such a runway would be very questionable, if not useless.

A complete study of this issue should include equivalent simulations for a typical airport, at which crosswinds past terminal buildings and hangars also generate turbulence that is more intense and more focused than the normal turbulence of the atmospheric boundary layer over a flat surface. These flows could contain stable vortices aligned with the wind, for instance. Such comparisons are left for future work.

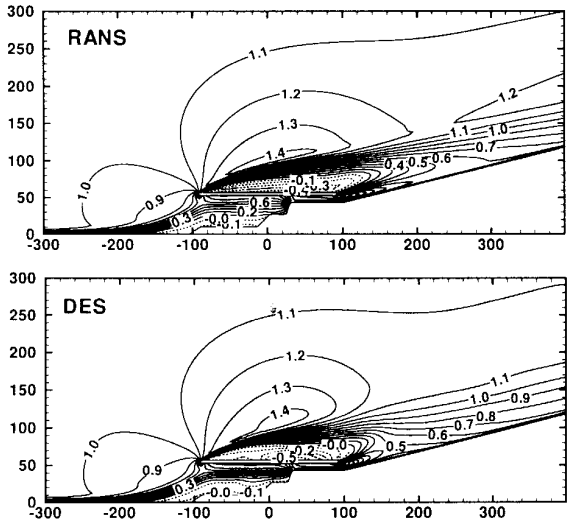

Fig. 27 Comparison of 2D RANS with time and span averaged DES velocity fields over the runway: contours of wind velocity.

3.3.4. Landing Gear Truck.

This is the first example of DES of a really complex 3D geometry (courtesy of B. Lazos at NASA) shown schematically in Fig.28 together with some elements of a thirteen-block structured grid. The total number of grid points is about $2.5 \cdot 10^6$.

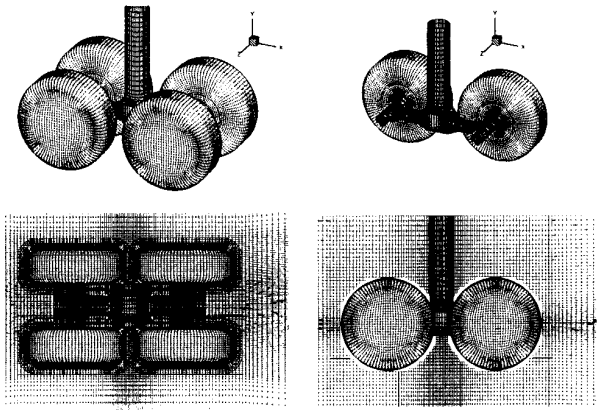

Fig. 28 Fragments of the 13-block computational grid used for DES of landing gear truck.

Extensive DES and URANS studies of this flow aimed, mostly, at resolving the unsteady flow physics in more detail for noise applications are currently in progress at Boeing and will be published soon.[43] Here we are presenting only some illustrations of the preliminary studies directed mostly to establishing the feasibility of DES as applied to this flow.

Figure 29 is a flow visualization in two planes which bisect the domain, obtained with the use of the fifth order upwind scheme. Just as in all the other cases

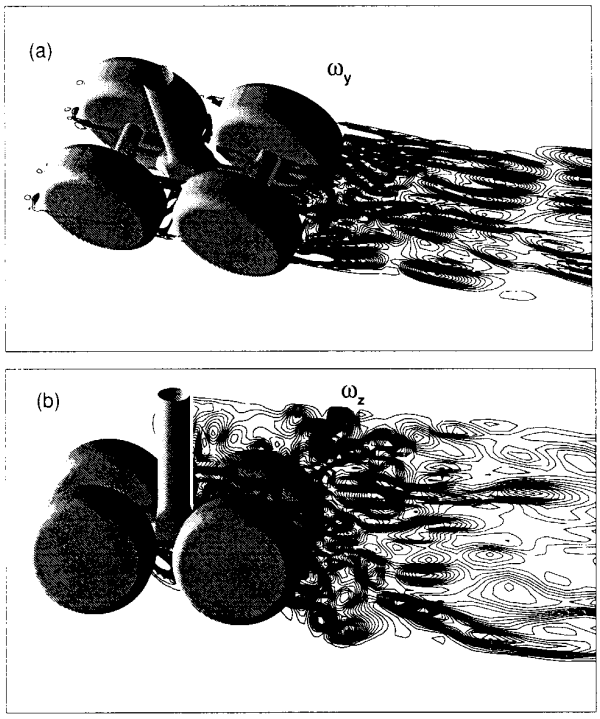

Fig. 29 Visualization of the landing gear flow (vorticity contours in horizontal and vertical planes at Re=100,000).

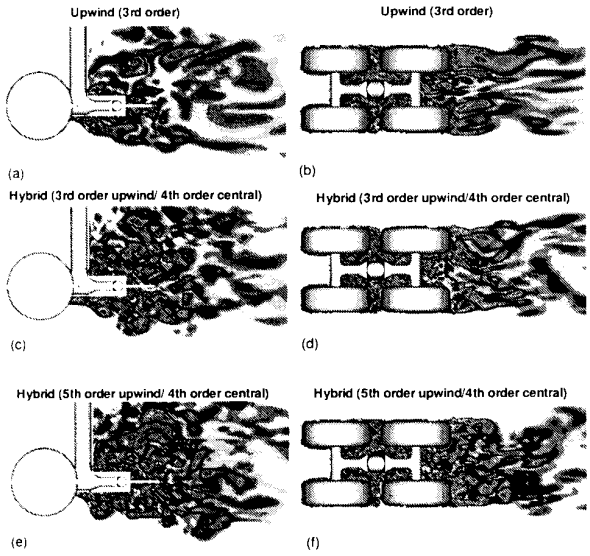

Fig. 30 Effect of the numerical method on the vorticity field in DES of the landing gear.

considered above, DES has finer structures than those of URANS, even with the same grid.[43]

Figure 30 demonstrates the effect of the numerical dissipation on the resolved flow pattern. In particular, it shows how the resolution improves with an increase of the upwind-scheme order of accuracy, and with a switch from the upwind to the hybrid scheme.

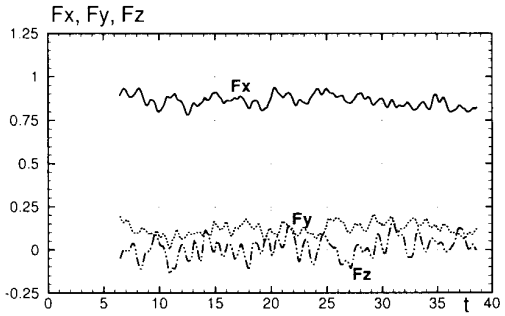

Fig. 31 Time-dependent forces on landing gear.

Therefore, at least as far as broadband-noise applications are concerned the less-dissipative high-order hybrid scheme is apparently preferable. However, for now, we do not yet have a definitive answer on how accurate the small eddies are, and whether they affect the unsteady landing gear forces shown in Fig.31 significantly.

4. Concluding Remarks.

In this paper we make an attempt to outline the reasoning behind and the emerging level of success of the Detached-Eddy Simulation of complex massively-separated turbulent flows at high Reynolds number. A wide range of computational examples is presented with the hope that they support the credibility of the approach and highlight both its strong points and "pacing items". Summarizing, it seems to be justified to state that until now no examples have been found where DES performed worse than steady or unsteady RANS, while a wide range of flows where DES is definitely superior over RANS does exist.

In terms of computational cost, the initial DES is shown to be affordable on personal computers even for complex wall-bounded flows, which are unreachable with LES when any of the boundary layers are turbulent. By "personal computers" we mean recent models in the 800Mhz range, and we accept that runs take weeks. By "initial DES" we mean one on a grid fine enough to support a fairly wide range of scales. A thorough study requires this initial run, and one with an unquestionable refinement of the grid in all four directions; the fine-grid run is not possible on personal computers for real-life geometries, and we consider that we have achieved this refinement only for the circular cylinder.[6]

The DES approach is still young and unresolved issues of course exist. Some are common with RANS, notably those of transition prediction and even of transition control within the turbulence model (once prediction is successful or a trip is used). We have covered those of the differencing scheme, and similar studies for time differencing may be in order. The conversion of a typical RANS code to DES is rapid as far as the modification of the model goes, but achieving the required

spatial and temporal accuracy for LES can demand deep improvements. It is also clear that grid design is a complex matter if an efficient use of all the grid points is to be made. Thus, DES can address some very challenging flow physics but the burden on the user is, not surprisingly, even higher than for a RANS study. This burden includes grid design and a careful scrutiny of the solution, often leading to grid re-design. Automatic adaptation appears to be a distant prospect (however, adaptation in any Navier-Stokes method appears to be in need of breakthroughs), and quantitative error estimates from a single solution, which would remove the need for grid refinement, are simply absent.

We also hope that the paper gives convincing physical arguments in favor of the statement that useful methods for high-Reynolds-number separated flows, even if they are not exactly DES, will all be a type of hybrid between RANS and LES.

Acknowledgements.

I am grateful to my friends and colleagues both in St.-Petersburg (Drs. M.Shur and A.Travin) and in Seattle (Drs. P.Spalart and L.Hedges), who all are in fact the coauthors of this paper, for the pleasure to work with them. My special gratitude is to P.Spalart, who encouraged me to work on the paper and improved the manuscript a lot. Drs. S.Allmaras and L.Hedges reviewed the manuscript. The work was supported by the Boeing Technology Research Center in Moscow and, partly, by the Russian Basic Research Foundation, grant 00-02-17184.

References

[1]Spalart, P.R., Jou, W.-H., Strelets, M., and Allmaras, S.R., "Comments on the feasibility of LES for wings, and on a hybrid RANS/LES approach", 1st AFOSR Int. Conf. on DNS/LES, Aug. 4–8, 1997, Ruston, LA. In Advances in DNS/LES, C.Liu & Z.Liu Eds., Greyden Press, Columbus, OH.

[2]Spalart, P.R., "Strategies for turbulence modelling and simulations", In: 4th Int. Symp. Eng. Turb. Modelling and Measurements, pp.3–17. May 24–24, 1999, Corsica, France

[3]Spalart, P.R., "Trends in Turbulence Treatments", 2000, AIAA Paper 2000-2306.

[4]Spalart, P.R., and Allmaras, S.R., "A one-equation turbulence model for aerodynamic flows", La Rech. A'erospatiale, 1994, V.1, pp.5–21.

[5]Menter,F.R., "Zonal two-equation k-omega turbulence models for aerodynamic flows", 1993, AIAA Paper 1993-2906.

[6]Travin, A., Shur, M., Strelets, M., and Spalart. P.R., "Detached-eddy simulations past a circular cylinder", Int. J. Flow, Turbulence and Combustion, 2000, V.63, Nos. 1–4, pp.293-313.

[7]Gulyaev, A.N., Kozlov, V.Ye., and Secundov, A.N., "A universal one-equation model for turbulent viscosity", Fluid Dynam., 1993, V.28, No.4, 484–494 [translated from Russian, Consultants Bureau, New York].

[8]Travin, A., Shur, M., Strelets, M., and Spalart. P.R., "Physical and numerical upgrades in the detached-eddy simulation of complex turbulent flows", 2000. In: 412 EUROMECH Colloquium on LES of Complex transitional and turbulent flows, Munich, Oct. 2000, Book of Abstracts.

[9]Comte-Bellot, G., and Corrsin, S., "Simple Eulerian time correlation of full- and narrow-band velocity signals in grid-generated 'isotropic' turbulence", J. Fluid Mech., 1971, V.48., pp.273–337.

[10]Constantinescu, G., and Squires, K.D., "LES and DES investigations of turbulent flow over a sphere", 2000, AIAA Paper 2000-0540.

[11]Shur, M., Spalart, P.R., Strelets, M., and Travin, A., "Detached-eddy simulation of an airfoil at high angle of attack". In: Rodi, W., and Laurence, D. (eds.) 4th Int. Symp. Eng. Turb. Modelling and Measurements, pp.669–678. May 24–24, 1999. Corsica, Elsevier, Amsterdam.

[12]Rogers, S.E., Kwak,D., "An upwind differencing scheme for the time-accurate incompressible Navier-Stokes equations", 1988, AIAA Paper 88-2583-CP.

[13]Forsythe, J., Hoffmann, K., and Dieteker, J.-F., "Detached-eddy simulation of a supersonic axisymmetric base flow with an unstructured flow solver", 2000, AIAA Paper 2000-2410.

[14]Moin, P., "Numerical and physical issues in large eddy simulation of turbulent flows", JSME Int. J., 1998, Series B, V.41, No.2, pp. 454–463.

[15]Nikitin, N.V., Nicoud, F., Wasistho, B., Squires, K.D., and Spalart P.R., "An approach to wall modelling in large-eddy simulation", Phys. Fluids., 2000, V.12, No.7.

[16]Shur, M.L., Spalart, P.R., Strelets, M.Kh., and Travin, A.K., "Navier-Stokes simulation of shedding turbulent flow past a circular cylinder and a cylinder with a backward splitter plate". In: Desideri, G.A., Hirsch, C., Le Tallec, P., Pandolfi, M., and Periaux, J. (eds), Third ECCOMAS CFD Conference, Paris, September, John Wiley & Sons, Chichester, 1996, pp. 676–682.

[17]Durbin, P.A., "Separated Flow Computations with the k-ϵ-v^2 model", AIAA J., 1995, V.33, No.4, 659–664.

[18]Abbott, I.H., and von Doenhoff, A.E., "Theory of wing sections, including summary of airfoil data". Dover, New York, 1959.

[19]McCroskey, W.J., "A Critical Assessment of Wind Tunnel Results for the NACA 0012 Airfoil". AGARD_CP429, 1987.

[20]McCroskey, W.J., McAlister, K.W., Carr, L.W., and Pucci, S.L., "An experimental study of dynamic stall on advanced airfoil sections", NASA TM 84245, 1982.

[21]Hoerner, S.F., "Fluid Dynamics Drag", 1958 http://members.aol.com/hfdy/home.htm

[22]Najjar, F.M., Vanka, S.P., "Effects of intrinsic three-dimensionality on the drag characteristics of a normal flat plate". Phys. Fluids, 1995, V.7, No.10, p.1216.

[23]Abernathy,F.H., "Flow over an inclined plate". ASME J. Basic Eng., 1962, V.61, pp.380–388.

[24]Breuer, M., "A challenging test case for large eddy simulation: high Reynolds number circular cylinder flow", Int. J. Heat and Fluid Flow, 2000, V.21, pp.648–654.

[25]Spalart, P.R., Strelets, M.Kh., "Mechanisms of transition and heat transfer in a separation bubble". J.Fluid Mech., 2000, V.403, pp.329–349.

[26]Perry, A.E., and Chong, M.S., "A study of edding motions and flow patterns using critical point concepts", 1994, Ann. Rev.Fluid Mech., V.258, 258–287.

[27]Najjar, F.M., Balachandar, S., "Low-frequency unsteadiness in the wake of a normal flat plate", J. Fluid Mechanics, 1998, V.370, p.101.

[28]Breuer, M., "Large eddy simulation of the subcritical flow past a circular cylinder: numerical and modeling aspects", Int. J. Numer. Methods Fluids, 1998, V.28, pp.1281-1302.

[29]Rodi, W., "Large-eddy simulation of the flows past bluff bodies". In: Launder, B.E. and Sandham, N.H. (eds.) Closure Strategies for Turbulent and Transitional Flows. Cambridge University Press, Cambridge, 2000.

[31] Humphreys, J.S., "On a circular cylinder in a steady wind at transition Reynolds numbers". J. Fluid Mech., 1960, V.9, pp. 603-612.

[32] Schewe, G., "On the force oscillations on a circular cylinder in cross flow from subcritical up to transitional Reynolds numbers". J. Fluid Mech., 1983, V.133, pp.265–285.

[33] Roshko, A., "Experiments on the flow past a circular cylinder at very high Reynolds number", J. Fluid Mech., 1961, V.10(3), pp.345–356.

[34] van Nunen, J.W.G., "Pressure and forces on circular cylinder in a cross flow at high Reynolds numbers." In: Naudascher, (ed.), Flow Induced Structural Vibrations. 1974, Springer-Verlag, Berlin, pp. 748–754.

[35] Jovic, S., and Driver, D., "Reynolds number effects on the skin friction in separated flows behind a backward facing step," 1995, Exp. Fluids, V.18, p.464.

[36] Shur, M., Strelets, M., Zaikov, L., Gulyaev, A., Kozlov, V., and Secundov, A., "Comparative numerical testing of one- and two-equation turbulence models for flows with separation and reattachment". AIAA-95-0863.

[37] Le, H., Moin, P., and Kim, J., "Direct numerical simulation of turbulent flow over a backward-facing step". Ninth Symp. on Turbulent Shear Flows, Kyoto, Japan, Aug. 1993, pp. 13-2-1–13-2-5.

[38] Neto, A.S., Grand, D., Metais, O., and Lesieur, M., "A numerical investigation of the coherent vortices in turbulence behind a backward-facing step". J. Fluid Mech., 1993, V.256, pp. 1–25.

[39] Fureby, C., "Large eddy simulation of rearward-facing step flow". AIAA J., 1999, V.37, No.11, pp.1401-1410.

[40] Johansson, S. H., Davidson, L., and Olsson, E. "Numerical simulation of vortex shedding past triangular cylinders at high Reynolds number using a k-ϵ turbulence model", Int. J. Numer. Meth. Fluids, 1993, V.16, p.859.

[41] Madabhushi, R.K., Choi, D., and Barber, T.J., "Unsteady Simulations of turbulent flow behind a triangular bluff body", 1987, AIAA Paper 97-3182.

[42] Sjunesson, A., Nelson, C., and Max, E., "LDA measurements of velocities and turbulence in a bluff body stabilized flame", 4th Int. Conf. on Laser Anemometry Advances and Applications, 1991, ASME, Cleveland, OH.

[43] Hedges, L., Travin, A., Spalart, P., 2000, Private communication.